Inorg. Chem. **2008**, *47*, 7262−7270

Energy Transfer and Tunable Luminescence Properties of Eu^{3+} in $TbBO_3$ Microspheres via a Facile Hydrothermal Process

Jun Yang, Cuimiao Zhang, Chunxia Li, Yingning Yu, and Jun Lin*

State Key Laboratory of Rare Earth Resource Utilization, Changchun Institute of Applied Chemistry, Chinese Academy of Sciences, Changchun 130022, and Graduate University of the Chinese Academy of Sciences, Beijing 100049, P. R. China

Received April 2, 2008

$Tb_{(1-x)}BO_3:xEu^{3+}$ ($x = 0-1$) microsphere phosphors have been successfully prepared by a simple hydrothermal process directly without further sintering treatment. X-ray diffraction (XRD), Fourier transform infrared spectroscopy (FTIR), thermogravimetric analysis (TGA), scanning electron microscopy (SEM), transmission electron microscopy (TEM), high-resolution transmission electron microscopy (HRTEM), selected area electron diffraction (SAED), photoluminescence (PL), low-voltage cathodoluminescence (CL), and time-resolved emission spectra as well as lifetimes were used to characterize the samples. The as-obtained phosphor samples present sphere-like agglomerates composed of nanosheets with highly crystallinity in spite of the moderate reaction temperature of 200 °C. Under ultraviolet excitation into the $4f^8 \rightarrow 4f^75d$ transition of Tb^{3+} at 245 nm (or 284 nm) and low-voltage electron beams' excitation, $TbBO_3$ samples show the characteristic emission of Tb^{3+} corresponding to $^5D_4 \rightarrow {}^7F_{6,\,5,\,4,\,3}$ transitions; whereas $TbBO_3:Eu^{3+}$ samples mainly exhibit the characteristic emission of Eu^{3+} corresponding to $^5D_0 \rightarrow {}^7F_{0,\,1,\,2,\,3,\,4}$ transitions due to an efficient energy transfer occurs from Tb^{3+} to Eu^{3+}. The increase of Eu^{3+} concentration leads to the increase of the energy-transfer efficiency from Tb^{3+} to Eu^{3+} but also enhances the probability of the interaction between neighboring Eu^{3+}, which results in the concentration quenching. The PL color of $TbBO_3:xEu^{3+}$ phosphors can be easily tuned from green, yellow, orange, to red-orange by changing the doping concentration (x) of Eu^{3+}, making the materials have potential applications in fluorescent lamps for advertizing signs and other color display fields.

1. Introduction

Inorganic phosphor materials based on rare earth (RE) compounds and RE ions doped compounds have been widely used in modern lighting and display fields, such as fluorescent lamps, cathode-ray tubes, field emission displays, and plasma display panels because of their abundant emission colors resulting from the 4f electronic shells.[1] Recently, the request for light-emitting-diode (LED) converted phosphors has triggered active research efforts in the investigation of single-phased light-emitting phosphors via chemical approaches.[2] It is well-known that the energy transfer plays an important role in luminescent materials both from theoretical and practical points of view.[1c,e] It has been recognized that the luminescence intensities of various rare earth ions can be enhanced or quenched by the energy transfer from other co-doped rare earth ions.[1c,3a] For example, the emission intensity of Tb^{3+} is greatly enhanced by an energy transfer from Ce^{3+} in $LaPO_4:Ce^{3+}$, Tb^{3+} phosphor, leading it to be an efficient luminescent material for fluorescent lamps.[1c] It has also been demonstrated that as a result of the energy transfer phenomena it is possible to reduce the threshold energy of laser oscillation in some solid laser materials.[3b] As the most frequently used activator ions in luminescent materials, the Eu^{3+} and Tb^{3+} mainly show emissions due to transitions of $^5D_0 \rightarrow {}^7F_J$ ($J = 1, 2, 3, 4$) in the red region and $^5D_4 \rightarrow {}^7F_J$ ($J = 6, 5, 4, 3$) in the green region, respectively.[1c] Moreover,

* To whom correspondence should be addressed. E-mail: jlin@ciac.jl.cn.

(1) (a) Yu, M.; Lin, J.; Fu, J.; Zhang, H. J. *J. Mater. Chem.* **2003**, *13*, 1413. (b) Capobianco, J. A.; Vetrone, F.; Boyer, J. C.; Speghini, A.; Bettinelli, M. *Opt. Mater.* **2002**, *19*, 259. (c) Blasse, G.; Grabmaier, B. C. *Luminescent Materials*; Springer-Verlag: Berlin, Heideberg, 1994. (d) Feldmann, C.; Jüstel, T.; Ronda, C. R.; Schmidt, P. J. *Adv. Funct. Mater.* **2003**, *13*, 511. (e) Evans, R. C.; Carlos, L. D.; Douglas, P.; Rocha, J. *J. Mater. Chem.* **2008**, *18*, 1100.

(2) (a) Yang, W. J.; Chen, T. M. *Appl. Phys. Lett.* **2006**, *88*, 101903. (b) Hayakawa, T.; Hiramitsu, A.; Nogami, M. *Appl. Phys. Lett.* **2003**, *82*, 2975.

10.1021/ic800586n CCC: $40.75
Published on Web 07/23/2008

it is well-known that an effective energy transfer can take place from Tb^{3+} to Eu^{3+} in several hosts, such as tungstates,[4a] zeolite-Y,[4b] yttria,[4c] porous silicon,[4d] and molybdates.[4e] In these works, there is a common feature that the Tb^{3+} and Eu^{3+} ions are codoped in the third-party hosts. So far, only limited information is available on Eu^{3+}-doped terbium-based hosts,[4f–h] whose crystal structures belong to both monoclinic and hexagonal respectively.

To obtain desired RE ions doped phosphors, wet chemistry processes, such as coprecipitation,[5a] hydrothermal synthesis,[5b–d] and colloidal chemistry[5e] are extensively used because starting materials in these methods can be mixed at molecular level and the reaction temperature for the formation of desired products is relatively low. However, most phosphors prepared from wet chemistry methods crystallize and exhibit luminescence only after being sintered at high temperature. This is because OH^- groups and/or crystal water molecules attached on the particle surface or in host lattice are unavoidable and may quench the luminescence. Consequently, further sintering these precursors at higher temperature is needed to improve the luminescence intensity in most cases.[4f,6] However, this can not work for those phosphors based on Tb^{3+}, which will be favored over Tb^{4+} at elevated temperature.

It is well-known that phosphors based on borates have attracted much attention due to their high stability, low synthesis temperature, and high ultraviolet and optical damage threshold.[7a–e] Rare earth orthoborates $LnBO_3$ (Ln = lanthanides and yttrium) have been proved to be very useful host lattices for the luminescence of Eu^{3+} and Tb^{3+}, which have been found wide applications in mercury-free fluorescent lamps and various kinds of display devices.[7f–h] For example, YBO_3:Eu^{3+} is currently used as a red component in PDP television. Up to now, there have been many reports about synthesis and luminescent properties of $LnBO_3$ and/or RE^{3+}-doped $LnBO_3$ materials except Ln = Pm, Tb, Ho, and Tm.[7h,8] Unfortunately, so far little attention has been paid to synthesis and luminescent properties of $TbBO_3$ and $TbBO_3$:Eu^{3+}, and the corresponding energy transfer from Tb^{3+} to Eu^{3+} in $TbBO_3$ host has not been realized and reported. $TbBO_3$ is of hexagonal crystal structure, which may be favorable for the energy transfer from Tb^{3+} to Eu^{3+}.[4f–h]

Accordingly in this article, we report the synthesis of $Tb_{(1-x)}BO_3$:xEu^{3+} ($x = 0-1$) microsphere phosphors directly by a simple hydrothermal method without further sintering treatment. The as-obtained products present sphere-like agglomerates composed of nanosheets. In spite of the moderate reaction temperature of 200 °C, the as-synthesized $TbBO_3$:xEu^{3+} is highly crystalline. Moreover, we investigated the energy transfer property from Tb^{3+} to Eu^{3+} in $TbBO_3$, and tunable emission colors were realized in these materials by changing the doping concentration of Eu^{3+}.

2. Experimental Section

Materials. The initial chemicals in this work, Tb_4O_7 and Eu_2O_3 (both with purity of 99.99%, Changchun Applied Chemistry Science and Technology Limited, China), HCl, H_3BO_3, $NH_3 \cdot H_2O$, and ethanol (all with purity of analytical reagent, Beijing Fine Chemical Company, China), were used without further purification.

Preparation. The $Tb_{(1-x)}BO_3$:xEu^{3+} ($x = 0-1$) samples were all prepared by a simple hydrothermal process. First, Tb_4O_7 and Eu_2O_3 were dissolved in dilute HCl respectively, resulting in the formation of a colorless stock solution of $TbCl_3$ with 0.2 mol/L and a colorless solution of $EuCl_3$ with 0.0002 and 0.02 mol/L. In a typical synthesis, the stoichiometric amounts of $TbCl_3$ solution, $EuCl_3$ solution, and H_3BO_3 (100% excess) were mixed under stirring, and then deionized water was added to the above mixture to reach 41 mL for total volume of H_2O. The solution was stirred for another 30 min to form a clear aqueous solution. Then 25 wt% of $NH_3 \cdot H_2O$ (A.R.) was introduced dropwise to the vigorously stirred solution until pH 8. After additional agitation for 40 min, the as-obtained white colloidal precipitate was transferred to a 50 mL autoclave, sealed, and heated at 200 °C for 24 h. It was then cooled to room temperature naturally. The products were then collected by filtration, washed with ethanol, and deionized water for several times, and dried in atmosphere at 100 °C for 6 h.

Characterization. The phase purity and crystallinity of the samples were examined by powder X-ray diffraction (XRD) performed on a Rigaku-Dmax 2500 diffractometer with Cu Kα radiation ($\lambda = 0.15405$ nm). Fourier transform infrared spectroscopy (FTIR) spectra were measured with PerkinElmer 580B infrared spectrophotometer with the KBr pellet technique. Thermogravi-

(3) (a) Nakazawa, E.; Shionoya, S. *J. Chem. Phys.* **1976**, *47*, 3211. (b) Johnson, L. P.; Geusic, J. E.; Van Uitert, L. C. *Appl. Phys. Lett.* **1966**, *8*, 200.

(4) (a) Holloway, W. W.; Kestigian, M.; Newman, R. *Phys. Rev. Lett.* **1963**, *11*, 458. (b) Chen, W.; Sammynaiken, R.; Huang, Y. *J. Appl. Phys.* **2000**, *88*, 1424. (c) Kim Anh, T.; Ngoc, T.; Thu Nga, P.; Bitch, V. T.; Long, P.; Strek, W. *J. Lumin.* **1988**, *39*, 215. (d) Moadhen, A.; Elhouichet, H.; Canut, B.; Sandu, C. S.; Oueslati, M.; Roger, J. A. *Mater. Sci. Eng., B* **2003**, *105*, 157. (e) Zhang, Z. J.; Chen, H. H.; Yang, X. X.; Zhao, J. T. *Mater. Sci. Eng., B* **2007**, *145*, 34. (f) Di, W. H.; Wang, X. J.; Zhu, P. F.; Chen, B. J. *J. Solid State Chem.* **2007**, *180*, 467. (g) Kim Anh, T.; Strek, W. *J. Lumin.* **1988**, *42*, 205. (h) Schierning, G.; Batentschuk, M.; Osvet, A.; Winnacker, A. *Radiat. Meas.* **2004**, *38*, 529.

(5) (a) Lind, C.; Wilkinson, A. P.; Rawn, C. J.; Payzant, E. A. *J. Mater. Chem.* **2001**, *11*, 3354. (b) Yang, J.; Liu, X. M.; Li, C. X.; Quan, Z. W.; Kong, D. Y.; Lin, J. *J. Cryst. Growth* **2007**, *303*, 480. (c) Li, Z. H.; Zeng, J. H.; Li, Y. D. *Small* **2007**, *3*, 438. (d) Meyssamy, H.; Riwotzki, K.; Kornowski, A.; Naused, S.; Haase, M. *Adv. Mater.* **1999**, *11*, 840. (e) Huignard, A.; Gacoin, T.; Boilot, J. P. *Chem. Mater.* **2002**, *12*, 1090.

(6) (a) Pan, Y. X.; Wu, M. M.; Su, Q. *Mater. Res. Bull.* **2003**, *38*, 1537. (b) Kutty, T. R. N.; Nayak, M. *Mater. Chem. Phys.* **2000**, *65*, 158.

(7) (a) Hao, J. H.; Gao, J.; Cocivera, M. *Appl. Phys. Lett.* **2003**, *82*, 2778. (b) Hao, J. H.; Gao, J.; Cocivera, M. *Appl. Phys. Lett.* **2003**, *82*, 2224. (c) Hao, J. H.; Cocivera, M. *Appl. Phys. Lett.* **2001**, *79*, 740. (d) Zeng, Q. H.; Pei, Z. W.; Wang, S. B.; Su, Q. *Spectrosc. Lett.* **1999**, *32*, 895. (e) Mikhaila, P.; Hulligera, J.; Ramseyerb, K. *Solid State Commun.* **1999**, *112*, 483. (f) Li, Z. H.; Zeng, J. H.; Chen, C.; Li, Y. D. *J. Cryst. Growth* **2006**, *286*, 487. (g) Chadeyron, G.; Mahiou, R.; EL-Ghozzi, M.; Arbus, A.; Zambon, D.; Cousseins, J. C. *J. Lumin.* **1997**, *72−74*, 564. (h) Mansuy, C.; Nedelec, J. M.; Dujardin, C.; Mahiou, R. *Opt. Mater.* **2007**, *29*, 697.

(8) (a) Zhang, J.; Lin, J. *J. Cryst. Growth* **2004**, *271*, 207. (b) Kim, T.; Kang, S. *Mater. Res. Bull.* **2005**, *40*, 1945. (c) Ma, J.; Wu, Q. S.; Ding, Y. P.; Chen, Y. *Cryst. Growth Des.* **2007**, *7*, 1553. (d) Giesber, H.; Ballato, J.; Chumanov, G.; Kolis, J.; Dejneka, M. *J. Appl. Phys.* **2003**, *93*, 8987. (e) Yin, M.; Corbel, G.; Leblanc, M.; Antic-Fidancev, E.; Krupa, J. C. *J. Alloys Compd.* **2000**, *302*, 12. (f) Huppertz, H.; von der Eltz, B.; Hoffmann, R. D.; Piotrowski, H. *J. Solid State Chem.* **2002**, *166*, 203. (g) Goubin, F.; Montardi, Y.; Deniard, P.; Rocquefelte, X.; Brec, R.; Jobica, S. *J. Solid State Chem.* **2004**, *177*, 89. (h) Laureiro, Y.; Veiga, M. L.; Fernández, F.; Saez-Puche, R.; Jerez, A.; Pico, C. *J. Less-Common Met.* **1991**, *167*, 387.

(9) (a) Yang, J.; Li, C. X.; Zhang, X. M.; Quan, Z. W.; Zhang, C. M.; Li, H. Y.; Lin, J. *Chem.—Eur. J.* **2008**, *14*, 4336. (b) Clark, B. L.; Keszler, D. A. *Inorg. Chem.* **2001**, *40*, 1724. (c) Wang, Y. H.; Wu, C. F.; Zhang, J. C. *Mater. Res. Bull.* **2006**, *41*, 1571. (d) Boyer, D.; Leroux, F.; Bertrand, G.; Mahiou, R. *J. Non-Cryst. Solids* **2002**, *306*, 110.

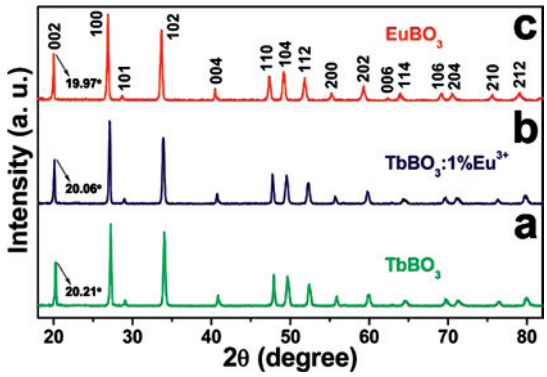

Figure 1. XRD patterns for $TbBO_3$ (a), $TbBO_3$:1%Eu^{3+} (b), and $EuBO_3$ (c) samples.

metric analysis (TGA) data were recorded with Thermal Analysis Instrument (SDT 2960, TA Instruments, New Castle, DE) with the heating rate of 10 °C·min^{-1} in a N_2 flow of 100 mL·min^{-1}. The morphology and structure of the samples were inspected using a field emission scanning electron microscopy (FE-SEM, XL 30, Philips) and a transmission electron microscope. Low-resolution transmission electron microscopy (TEM) images and selective area electron diffraction (SAED) patterns were obtained using a JEOL 2010 transmission electron microscope operating at 150 kV. High-resolution transmission electron microscopy (HRTEM) images were performed using FEI Tecnai G2 S-Twinwere with a field emission gun operating at 200 kV. Images were acquired digitally on a Gatan multiple CCD camera. Photoluminescence (PL) excitation and emission spectra were recorded with a Hitachi F-4500 spectrophotometer equipped with a 150 W xenon lamp as the excitation source at room temperature. The cathodoluminescent (CL) measurements were carried out in an ultrahigh-vacuum chamber ($<10^{-8}$ torr), where the samples were excited by an electron beam at a voltage range of 1∼5 kV with different filament currents, and the spectra were recorded on an F-4500 spectrophotometer. The luminescence decay curves and the time-resolved emission spectrum were obtained from a Lecroy Wave Runner 6100 Digital Osilloscope (1 GHz) using a tunable laser (pulse width = 4 ns, gate = 50 ns) as the excitation (Contimuum Sunlite OPO). All of the measurements were performed at room temperature.

3. Results and Discussion

Structure and Morphology. Parts a−c of Figure 1 show the XRD patterns of $TbBO_3$, $TbBO_3$:1%Eu^{3+}, and $EuBO_3$ samples, respectively. Both $TbBO_3$ and $EuBO_3$ exhibit very similar X-ray diffraction patterns with hexagonal-vaterite structure (parts a and c of Figure 1) so that we can expect their full miscibility. Therefore, the whole solid solution $Tb_{1-x}BO_3$:xEu^{3+} from $x = 0$ to 1 is expected to form. The calculated lattice constants using Jade 5.0 program, $a = b = 3.792$ Å, $c = 8.840$ Å for $TbBO_3$, $a = b = 3.805$ Å, $c = 8.865$ Å for $TbBO_3$:1% Eu^{3+}, and $a = b = 3.837$ Å, $c = 8.922$ Å for $EuBO_3$ are well compatible with the literature values from the standard card (JCPDS No. 24−1272 and 13−0485). It is worth noting that when the Tb^{3+} was substituted by the Eu^{3+}, the lattice constants become a little bigger and the corresponding XRD peaks move to a lower degree (arrows in Figure 1). No additional peaks of other phases have been found, indicating that Eu^{3+} has been effectively built into the $TbBO_3$ host lattice (part b of Figure 1). The relative intensity ratio of the diffraction peaks (002)

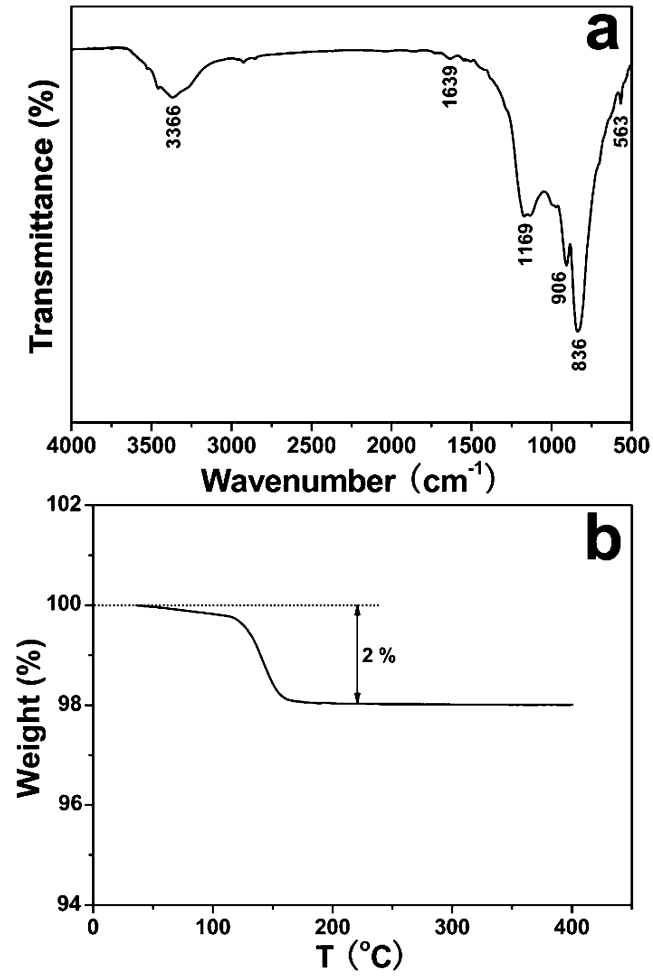

Figure 2. FTIR spectrum (a) and TGA curve (b) for $TbBO_3$:1% Eu^{3+} sample.

for $TbBO_3$, $TbBO_3$:1%Eu^{3+}, and $EuBO_3$ products is much higher than the conventional value (JCPDS No. 24−1272 and 13−0485, not shown here due to the limited space), indicating that the samples tend to be preferentially oriented due to the natural growing habit of forming 2D morphology during growth process of rare earth orthoborates.[8a,9a] What is more, high crystallinity can be obtained at a relatively low temperature.[9b] This is important for phosphors, because high crystallinity always means less traps and stronger luminescence. In addition, Tb^{3+} compound was prepared through hydrothermal process without reductive ambience for protection.

Part a of Figure 2 shows IR spectrum of $TbBO_3$:1% Eu^{3+} sample. There is a group of bands in the region 800−1200 cm^{-1} in vaterite-type borates. The IR spectrum of our present sample was in accordance with the references.[9c] Accordingly, the intense absorption band extending from 800 to 1200 cm^{-1} (peaks at 836, 906, and 1169 cm^{-1}) can be ascribed to a vaterite-type borate. A small peak near 563 cm^{-1} can be distinguished as an in-plane blending of the BO_4 group or the BO_3 group in vaterite-type borates. This is in good accordance with the XRD result above. The peaks of 3366 and 1639 cm^{-1} are ascribed to the OH stretching vibration mode and the HOH bending vibration mode of the H_2O molecule, respectively. The existence of water may arise

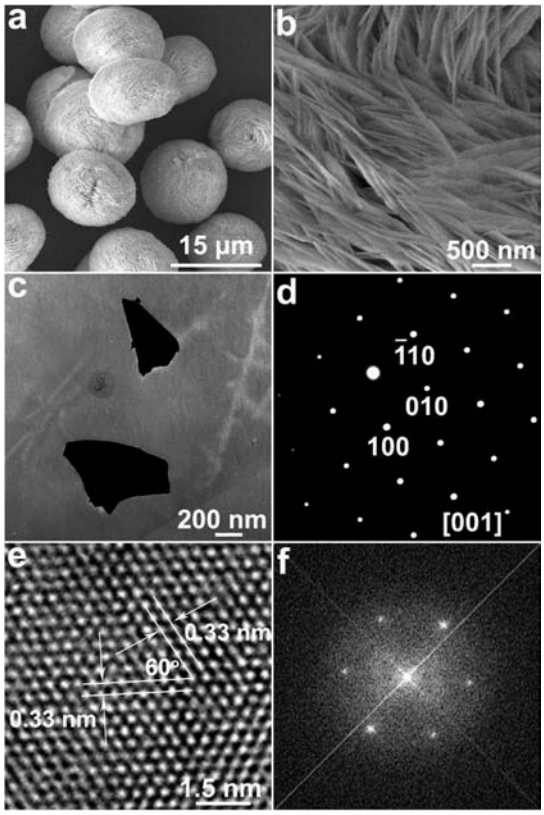

Figure 3. SEM images of the $TbBO_3$:1%Eu^{3+} sample (a, b), representative TEM image of the $TbBO_3$:1% Eu^{3+} nanosheets shed from the microspheres after ultrasonic treatment for 30 minutes (c), the corresponding electron diffraction pattern (d), HRTEM image of the broken nanosheet shown in part c (e), as well as the corresponding fast Fourier transform algorithm (FFT) image of part e (f).

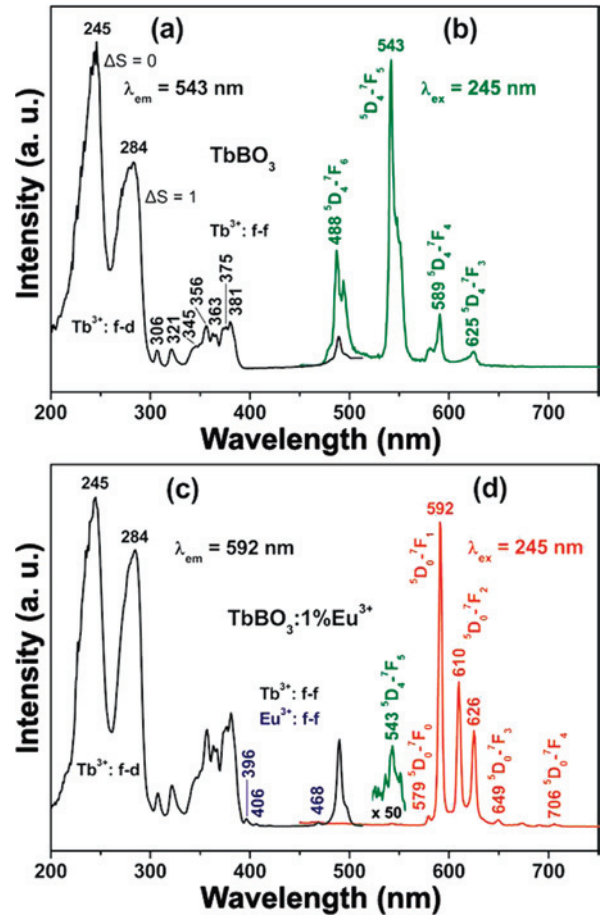

Figure 4. Excitation (a, c) and emission (b, d) spectra of the $TbBO_3$ (a, b) and $TbBO_3$:1%Eu^{3+} (c, d).

from residual water in the sample and/or absorbed moisture during the measurement. For precise estimate the proportion of water in the sample, we did TG analysis as shown in part b of Figure 2. The weight loss of 2% before 180 °C is due to evaporation of weakly bonded molecules, that is, residual water molecules attached on the particle surface in the sample.[9d] Generally, most phosphors prepared from wet chemistry methods crystallize and exhibit luminescence only after being sintered at high temperature. In our present work, we do not further calcine the hydrothermal products at high temperature for two reasons: (1) the $TbBO_3$:Eu^{3+} samples obtained through hydrothermal process have high crystallinity (Figure 1) and they have relative strong luminescence intensity (Figure 4); (2) Tb^{3+}-based host was prepared through hydrothermal process without reductive ambience for protection (while Tb^{3+} will be oxidized to Tb^{4+} at elevated temperature). This is also one of the merits for preparation of $TbBO_3$:Eu^{3+} phosphors via the hydrothermal process.

The SEM images of the $TbBO_3$:1%Eu^{3+} sample are shown in parts a and b of Figure 3, which exhibit that the sample consists of microspheres with diameter of about 15 μm, each of which is constructed by densely packed nanosheets with thickness of about 25 nm. Detailed surface observation (part b of Figure 3) implies that most of the nanosheets are linked together by both edge-to-edge and edge-to-surface conjunctions; the nanosheets extend outward from the center of the microstructure, and a few of them attach to each other. Therefore, such an architecture is a result of some type of self-assembly.[9a,10]

To further study the fine structure of the above microspheres, TEM was performed. Part c of Figure 3 shows a broken flake of the sphere obtained by ultrasonic treatment for about 30 minutes. These nanosheets are several hundred nanometers in the planar dimensions with smooth surfaces. The corresponding SAED pattern of the broken nanosheet taken along [001] zone axis shown in part d of Figure 3 reveals that the nanosheet ED pattern is characteristic of a hexagonal $TbBO_3$:Eu^{3+}, in good accordance with the XRD result. Moreover, SAED patterns taken from both different areas on a single fragment and different fragments were found to be identical within experimental accuracy, indicating that the $TbBO_3$:Eu^{3+} nanosheets are single-crystalline and that different nanosheets have identical crystallization habits. The patterns also reveal that the nanosheetes are stable enough to withstand the irradiation of convergent high-energy electron beams. Part e of Figure 3 is a high-resolution TEM image of the $TbBO_3$:1%Eu^{3+} nanosheets, which was taken with electron beam along [001] zone axis, perpendicular to the wide surface of the sheet. The lattice fringes show the imaging characteristics of the hexagonal $TbBO_3$ crystal, in

(10) Zhang, N.; Bu, W. B.; Xu, Y. P.; Jiang, D. Y.; Shi, J. L. *J. Phys. Chem. C* **2007**, *111*, 5014.

which the *d* spacing of 0.33 nm corresponds to the distance of the (100) planes. Further analysis indicates that the $TbBO_3$:Eu^{3+} nanosheet grows along the [100] or [010] crystallographic direction and is enclosed by ± (001) facets,[11] that is, the widest facets, as suggested in the XRD measurement. The corresponding fast Fourier transform algorithm (FFT) image (part f of Figure 3) shows the nature of 2D structure of hexagonal $TbBO_3$:Eu^{3+} nanosheets.

Luminescence Properties. Photoluminescence Properties. The $TbBO_3$ sample emits bright-green light under UV excitation. Figure 4 shows the excitation (a) and emission (b) spectra of the sample. The excitation spectrum of $TbBO_3$ monitored with 543 nm emission of Tb^{3+} ($^5D_4 \rightarrow {}^7F_5$) consists two main features, a broad structured plateau with maxima at 245 and 284 nm in the range of 200−300 nm, corresponding to spin-allowed $4f^8 \rightarrow 4f^75d^1$ ($^7F_6 \rightarrow {}^7D$) transition with higher energy (245 nm, $\Delta S = 0$) and spin-forbidden $4f^8 \rightarrow 4f^75d^1$ ($^7F_6 \rightarrow {}^9D$) transition with lower energy (284 nm, $\Delta S = 1$) of Tb^{3+} ion, respectively;[4b,12] and the characteristic f → f transition lines within the Tb^{3+} $4f^8$ configuration in the longer wavelength region, assigned as the transitions from the $^7F_6$ ground state to the different excited states of Tb^{3+}, that is, 306 nm ($^5H_6$), 321 nm ($^5D_0$), 345 nm ($^5G_2$), 356 nm ($^5D_2$), 363 nm ($^5L_{10}$), 375 nm ($^5G_6$), 381 nm ($^5D_3$), and 488 nm ($^5D_4$), respectively.[13] Note that the $\Delta S = 1$ component is 5600 cm^{-1} below the $\Delta S = 0$ component for the Tb^{3+} $4f^8 \rightarrow 4f^75d^1$ transition, basically agreeing with the literature values (5800−6000 cm^{-1}) in the oxide host lattices.[12c,d] Upon excitation into the $4f^8 \rightarrow 4f^75d^1$ transition at 245 nm (or 284 nm), the obtained emission spectrum (part b of Figure 4) of $TbBO_3$ consists of f → f transition lines within $4f^8$ electron configuration of Tb^{3+}, that is, $^5D_4 \rightarrow {}^7F_6$ (488 nm) in the blue region and $^5D_4 \rightarrow {}^7F_5$ (543 nm) in the green region, as well as $^5D_4 \rightarrow {}^7F_4$ (589 nm) and $^5D_4 \rightarrow {}^7F_3$ (625 nm) in the red region. The strongest one is located at 543 nm corresponding to $^5D_4 \rightarrow {}^7F_5$ transition of Tb^{3+}. The decay curve (part a of Figure 5) for the luminescence of Tb^{3+} (monitored by $^5D_4 \rightarrow {}^7F_5$, 543 nm) can be well fitted into single exponential function as $I = I_o \exp(-t/\tau)$ (where τ is the 1/*e* lifetime of the Tb^{3+} ion), and the lifetime τ for the $^5D_4$ state of Tb^{3+} is determined to be 0.18 ms in $TbBO_3$ sample.

However, the green emission of the $TbBO_3$ host material changes greatly when doping Eu^{3+} in it. The $TbBO_3$:1%Eu^{3+} sample shows a red-orange emission under UV excitation. Figure 4 shows the excitation (c) and emission (d) spectra of the sample. The excitation spectrum recorded at the 592 nm ($^5D_0 \rightarrow {}^7F_1$) of Eu^{3+} is composed exclusively of the excitation bands of Tb^{3+}, which is identical with the excitation spectrum of Tb^{3+} in $TbBO_3$ (part a of Figure 4), except for some minor f → f transition lines within the Eu^{3+} $4f^6$ configuration (396 nm, $^7F_0 \rightarrow {}^5L_6$; 406 nm, $^7F_0 \rightarrow {}^5D_3$; and 468 nm, $^7F_0 \rightarrow {}^5D_2$, as assigned in part c of Figure 4). Although in general there exists a charge transfer band of Eu^{3+}−O^{2-} around 250 nm for Eu^{3+} in the rare earth orthoborates $LnBO_3$ (Ln = Lu and Y),[7a–g,9a] here it is strongly overwhelmed by the absorption of the $4f^8 \rightarrow 4f^75d^1$ transition of Tb^{3+} in $TbBO_3$ host lattice. The presence of the excitation bands and lines of Tb^{3+} in the excitation spectrum monitored with Eu^{3+} emission clearly indicates that an energy transfer has occurred from Tb^{3+} to Eu^{3+} in the $TbBO_3$:1%Eu^{3+} sample. Excitation into the $4f^8 \rightarrow 4f^75d^1$ transition of Tb^{3+} excitation band at 245 nm (or 284 nm) yields mainly the emission of Eu^{3+} ($^5D_0 \rightarrow {}^7F_0$ at 579 nm, $^5D_0 \rightarrow {}^7F_1$ at 592 nm, $^5D_0 \rightarrow {}^7F_2$ at 610 and 626 nm, $^5D_0 \rightarrow {}^7F_3$ at 649 nm, and $^5D_0 \rightarrow {}^7F_4$ at 706 nm), together with the very weak emission of Tb^{3+} ($^5D_4 \rightarrow {}^7F_5$ at 543 nm, which only can be seen in the figure magnified to 50 times, green line), as shown in part d of Figure 4. This is further indicative of the energy transfer from Tb^{3+} to Eu^{3+} in $TbBO_3$:1%Eu^{3+} sample. Similar to the single exponential luminescence decay of Tb^{3+} in $TbBO_3$ sample, the luminescence decay curve of Tb^{3+} (part b of Figure 5) in the $TbBO_3$:1%Eu^{3+} sample can also be well fitted into single exponential function, and the lifetime τ for the $^5D_4$ state of Tb^{3+} is determined to be 0.003 ms in the $TbBO_3$:1%Eu^{3+} sample, which is much shorter than that in $TbBO_3$ (0.18 ms). Obviously, the shortening of the lifetime in $TbBO_3$:1%Eu^{3+} with respect to $TbBO_3$ is due to the occurrence of the energy transfer from Tb^{3+} to Eu^{3+} in the former sample.[4f–h]

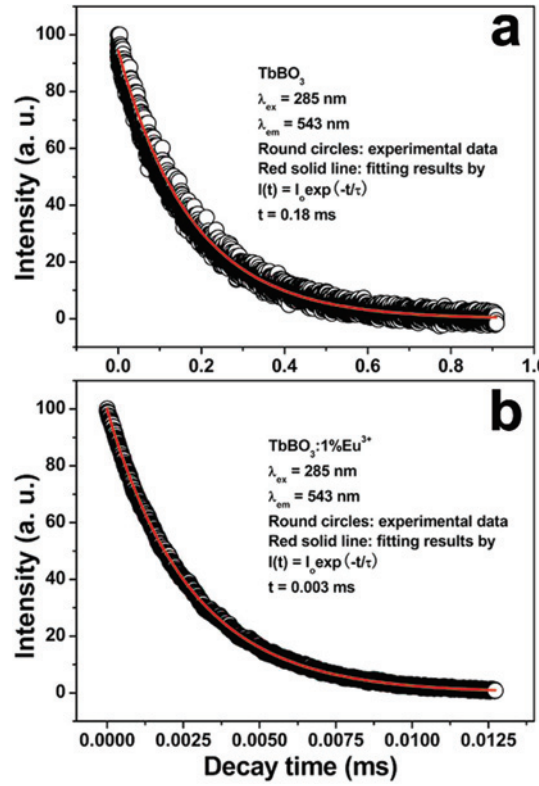

Figure 5. The decay curves for the luminescence of Tb^{3+} in $TbBO_3$ (a) and $TbBO_3$:1% Eu^{3+} (b).

Figure 6 shows the emission spectra of $TbBO_3$:xEu^{3+} (x = 0−1%) under 245 nm excitation. In the undoped $TbBO_3$ (x = 0), only the characteristic emissions of Tb^{3+} are

(11) Hu, J. Q.; Bando, Y.; Zhan, J. H.; Li, Y. B.; Sekiguchi, T. *Appl. Phys. Lett.* **2003**, *83*, 4414.
(12) (a) Zych, E. *Opt. Mater.* **2001**, *16*, 445. (b) Zycha, E.; Trojan-Piegza, J.; Hreniak, D.; Strek, W. *J. Appl. Phys.* **2003**, *94*, 1318. (c) Lin, J.; Su, Q. *J. Mater. Chem.* **1995**, *5*, 1151. (d) Blasse, G.; Bril, A. *Philips Res. Rep.* **1967**, *22*, 481.
(13) Thomas, K. S.; Singh, S.; Dieke, G. H. *J. Chem. Phys.* **1963**, *38*, 2180.

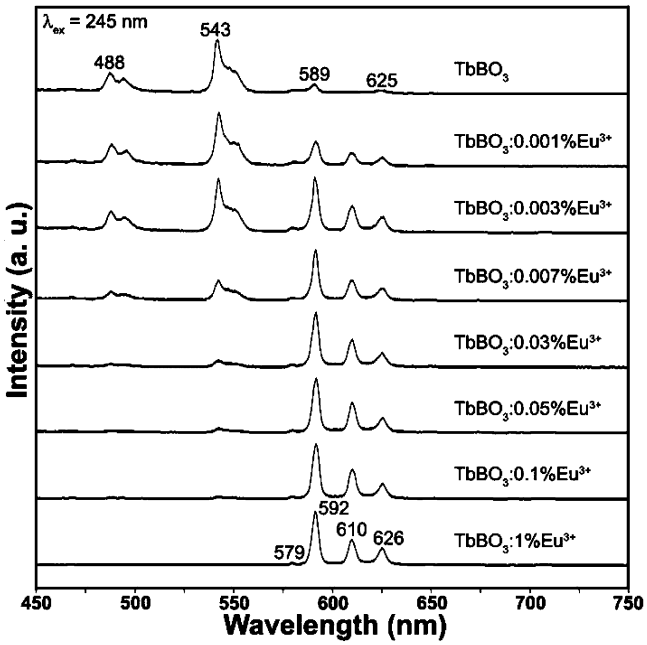

Figure 6. Emission spectra of the $TbBO_3$:xEu^{3+} samples with different concentration ($x = 0-1\%$) under 245 nm excitation.

Table 1. Energy Transfer Efficiency (η_{ET}) from Tb^{3+} to Eu^{3+}, the Life Time τ for the Luminescence of Tb^{3+}, Integrated Emission Intensity of Tb^{3+} and Eu^{3+} in the $TbBO_3$:xEu^{3+} ($x = 0-1\%$) Samples upon Excitation into the Tb^{3+} Excitation Band with 245 nm

	x							
	0	0.001%	0.003%	0.007%	0.03%	0.05%	0.1%	1%
I (Tb^{3+})	7102	11 107	10 706	8017	5593	3899	2591	926
I (Eu^{3+})		3318	5959	8855	19 901	19 436	19 326	18 433
τ (ms)	0.18	0.09	0.08	0.06	0.04	0.03	0.02	0.003
η_{ET} (%)		50	55	66	78	83	89	98

observed. With the doping of Eu^{3+} ($x = 0.001\%$), besides Tb^{3+} emissions, we can also observe the characteristic emissions of Eu^{3+}. With the increase of Eu^{3+} concentration, the luminescence of Tb^{3+} begins to decrease (Table 1), and that of Eu^{3+} increases first, both due to the enhancing the probability of energy transfer from Tb^{3+} to Eu^{3+} along with the increase of Eu^{3+} concentration. The luminescence of Eu^{3+} reaches the maximum at $x = 0.03\%$, and then begins to decrease (Table 1) due to the concentration quenching effect.[4f] This effect can be confirmed by the fluorescent dynamics of Eu^{3+}, as shown in Figure 7, from which a faster fluorescence decay of $^5D_0$ state of Eu^{3+} in $TbBO_3$:5% Eu^{3+} (2.45 ms) is observed than that in $TbBO_3$: 0.03%Eu^{3+} (2.91 ms). All results above indicate an efficient energy transfer from Tb^{3+} to Eu^{3+}. Also, such energy transfer behavior shows that the as-synthesized $TbBO_3$:Eu^{3+} is not a mixture of $TbBO_3$ and $EuBO_3$, but a solid solution, in which Eu^{3+} has successfully incorporated into $TbBO_3$ lattice.[4f] Otherwise, the $Tb^{3+} \rightarrow Eu^{3+}$ energy transfer can not occur in the separated phases. The energy transfer efficiency from Tb^{3+} to Eu^{3+} depends strongly on the doping concentration of Eu^{3+} in $TbBO_3$ host, just like that of $LaPO_4$:Ce^{3+}, Tb^{3+}.[14] The energy transfer efficiency from a donor (Tb^{3+}) to an acceptor (Eu^{3+}) can be calculated according to the formula $\eta_{ET} = 1 - I_d/I_{do}$ ($= 1 - \tau/\tau_o$), where I_d (τ) and I_{do} (τ_o) are the corresponding luminescence intensities (lifetimes) of the donor (Tb^{3+}) in the presence and absence of the acceptor (Eu^{3+}) for the same donor concentration (here, we overlooked tiny change of the donor (Tb^{3+}) concentration), respectively.[14] We investigated systematically the energy transfer efficiencies of $Tb^{3+} \rightarrow Eu^{3+}$ in $TbBO_3$:xEu^{3+} ($x = 0-1\%$) systems by calculating the lifetimes of Tb^{3+}, and the results are listed in Table 1. Clearly, it is known from Table 1 that with the increase of Eu^{3+} concentration, the energy transfer efficiency from Tb^{3+} to Eu^{3+} increases gradually. This is because the energy transfer probability from Tb^{3+} to Eu^{3+} is proportional to R^{-6} (R is the average distance between Tb^{3+} and Eu^{3+}).[15] When the Eu^{3+} concentration is equal to 1% mol of Tb^{3+}, η_{ET} reaches the value as high as 98%, but the emission of Eu^{3+} is not the strongest because the concentration quenching has occurred at this relative high concentration. The strongest emission was observed when the Eu^{3+} concentration is around 0.03% mol with an energy transfer efficiency from Tb^{3+} to Eu^{3+} of 78%.

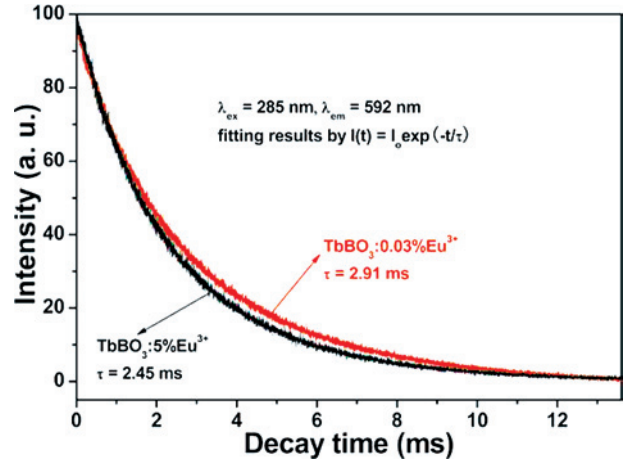

Figure 7. Decay curves for the luminescence of Eu^{3+} in the $TbBO_3$:0.03% Eu^{3+} and $TbBO_3$:5%Eu^{3+}.

The PL color can be tuned from green, yellow, orange, to red-orange by changing the doping concentration of Eu^{3+} ions due to different energy transfer efficiencies at different Eu^{3+} concentration. Part a of Figure 8 shows the corresponding CIE chromaticity diagram of $TbBO_3$:xEu^{3+} ($x = 0-1\%$) phosphors with different doping concentration of Eu^{3+} ions. The black dots indicate the CIE chromaticity coordinate positions. The CIE chromaticity coordinates change from $x = 0.2573$ $y = 0.4384$ for $TbBO_3$ to $x = 0.5655$ $y = 0.3589$ for $TbBO_3$:1%Eu^{3+} (labeled in part a of Figure 8 with an arrow) by changing the doping concentration of Eu^{3+} from $x = 0$ to 1% in $TbBO_3$:xEu^{3+} phosphors. The corresponding luminescence color can be changed from green, yellow, orange, to red-orange, which can be seen clearly from the photographs of the $TbBO_3$:xEu^{3+} samples presented in part b of Figure 8 where a 254 nm UV lamp was used as an excitation source and the samples were put onto filter paper in a dark room.

(14) Yu, M.; Lin, J.; Fu, J.; Han, Y. C. *Chem. Phys. Lett.* **2003**, *371*, 178.

(15) Riwotzki, K.; Meyssamy, H.; Kornowski, A.; Haase, M. *J. Phys. Chem. B* **2000**, *104*, 2824.

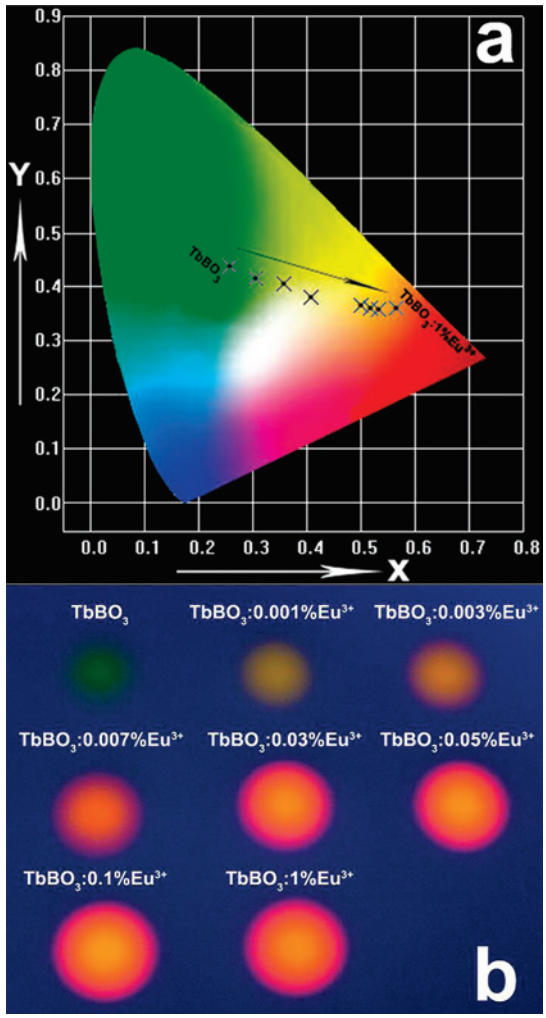

Figure 8. CIE chromaticity diagram (a) and the luminescent photographs (b) for the $TbBO_3$:xEu^{3+} samples ($x = 0-1\%$). Here, a 254 nm ultraviolet lamp was used as an excitation source, and the samples were put onto filter paper in a dark room.

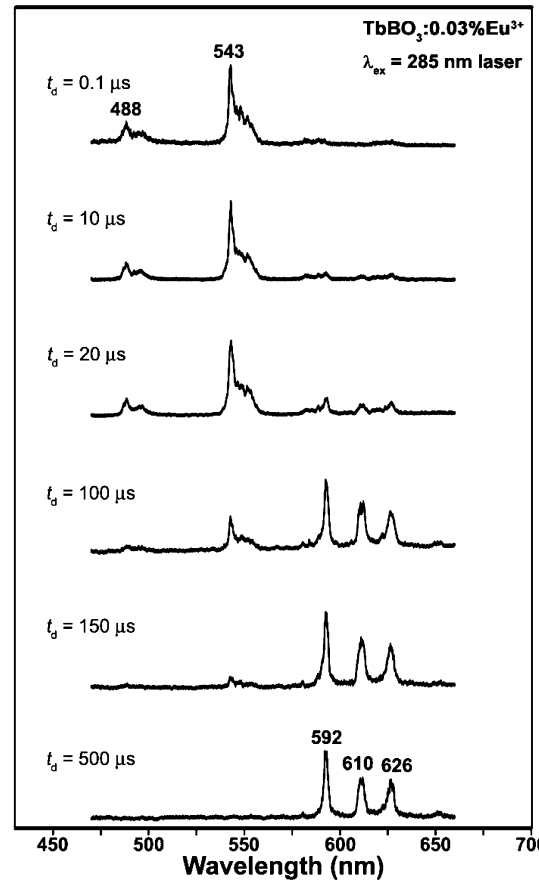

Figure 9. Time-resolved PL spectra of the $TbBO_3$:0.03%Eu^{3+} sample (λ_{ex} = 285 nm laser).

To study the energy transfer process from Tb^{3+} to Eu^{3+} in $TbBO_3$:Eu^{3+} in more detail, time-resolved emission spectra of $TbBO_3$:0.03%Eu^{3+} were measured by excitation into the Tb^{3+} band with a 285 nm laser. The emission spectra collected at different delay times (t_d) are shown in Figure 9. When $t_d = 0.1$ μs, only the characteristic emission of Tb^{3+} is observed; no Eu^{3+} emission is present because the excitation energy of Tb^{3+} has not been transferred to Eu^{3+} within this short time. When $t_d = 10$ μs, the emission of Tb^{3+} starts to decrease accompanied by the presence of Eu^{3+} emissions due to the energy transfer from Tb^{3+}. The emission of Tb^{3+} decreases gradually with further increase of the delay time, whereas that of Eu^{3+} begins to increase due to transfer of more excitation energy from Tb^{3+} to Eu^{3+}. When $t_d = 500$ μs, the emission of Tb^{3+} disappears, and the emission spectrum contains exclusively that of Eu^{3+}. When $t_d > 500$ μs, the Eu^{3+} emission also begins to decay gradually and disappears finally due to the depopulation of the excited states (figures are not shown due to the limited space). Actually, we cannot conclude whether the energy transfer from Tb^{3+} to Eu^{3+} is of radiative type or nonradiative type just from the time-resolved emission spectra shown in Figure 9. In general, radiative energy transfer only occurs in some crystals and the energy transfer among rare earth ions is of nonradiative type, that is, the resonant energy transfer occurs via the electric dipole−dipole or electric dipole−quadrupole interactions.[1c,3a] The same situation (nonradiative energy transfer) also holds for the energy transfer from Tb^{3+} to Eu^{3+} in our present work, which was well demenstrated in other hosts in previous reports.[4]

A summary of the emission and energy transfer process of Tb^{3+} and Eu^{3+} in $TbBO_3$:Eu^{3+} is shown schematically in Figure 10.[4] First, electrons on Tb^{3+} ions are excited from the ground state ($4f^8$) to the excited state ($4f^75d$) by UV light. Subsequently, these electrons relax to the lowest excited state $^5D_4$ through multiphonon relaxation then either return to the ground state to produce the Tb^{3+} emissions ($^5D_4 \rightarrow {}^7F_{6,5,4,3}$), or transfer their excitation energy from $^5D_4$ (Tb^{3+}) level to the higher excited energy levels of Eu^{3+} ($4f^6$) through cross relaxation, which relax to the $^5D_0$ (Eu^{3+}) level, where the red-orange emission ($^5D_0 \rightarrow {}^7F_{0,1,2,3,4,5,6}$) takes place. Because the $^5D_4 \rightarrow {}^7F_{6,5,4,3}$ emission of Tb^{3+} is effectively overlapped with the $^7F_{0,1} \rightarrow {}^5D_{0,1,2}$ absorption of Eu^{3+}, the energy transfer from Tb^{3+} to Eu^{3+} is very efficient in general.[16] Moreover, the hexagonal crystal structure of $TbBO_3$ also favors the energy transfer from Tb^{3+} to Eu^{3+}.[4f–h]

According to the model we proposed above, if Tb^{3+} ion was excited from $^7F_6 \rightarrow {}^5D_4$, there should be energy transfer

(16) Nakazawa, E.; Shionoya, S. *J. Chem. Phys.* **1967**, *47*, 3211.

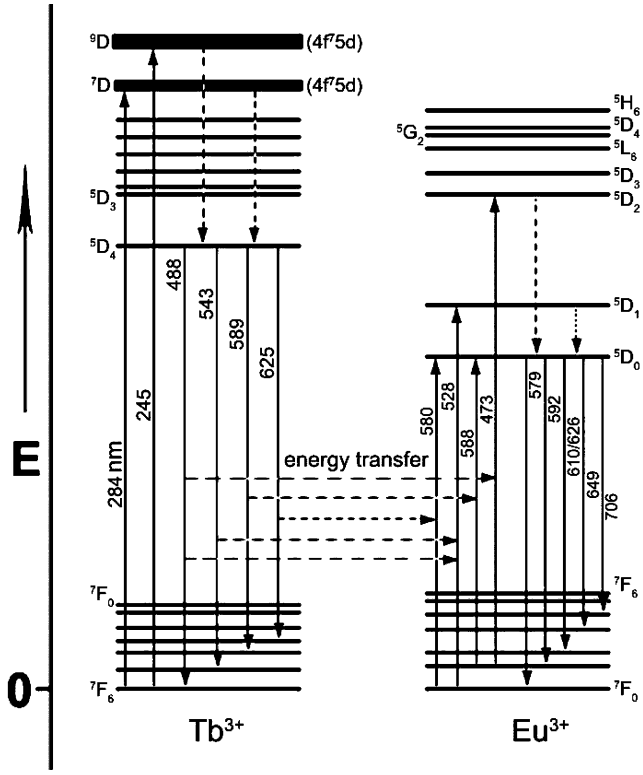

Figure 10. Scheme of energy transfer from Tb^{3+} to Eu^{3+}. The up solid arrows represent photoexcitation, the down solid arrows mean emission, and the down dash arrows denote multiphonon relaxation.

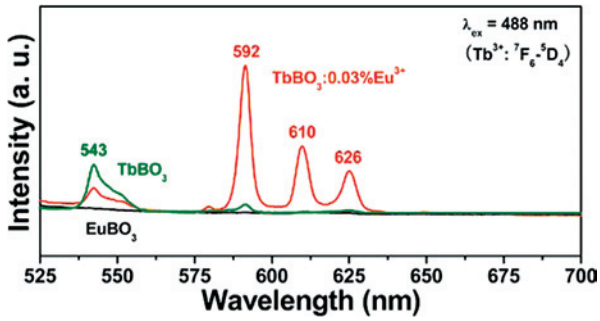

Figure 11. Emission spectra of the $TbBO_3$:0.03%Eu^{3+}, $TbBO_3$, $EuBO_3$ samples upon excitation into the $^7F_6 \rightarrow {}^5D_4$ transition of Tb^{3+} at 488 nm, respectively.

from the excited $^5D_4$ level of Tb^{3+} to the $^5D_{0,\,1,\,2}$ level of Eu^{3+} in $TbBO_3$:Eu^{3+} sample. Upon excitation into the $^7F_6 \rightarrow {}^5D_4$ transition of Tb^{3+} at 488 nm, the emission spectra of $TbBO_3$:0.03%Eu^{3+}, $TbBO_3$, and $EuBO_3$ are presented in Figure 11 for comparison. The emission spectrum of the $TbBO_3$:0.03%Eu^{3+} sample obtained by excitation with 488 nm ($^7F_6 \rightarrow {}^5D_4$ of Tb^{3+}) has principally the same feature as that of monitoring at 245 nm (Figure 6), and no emission is observed for pure $EuBO_3$. This further demonstrates that Tb^{3+} ion may act as a good energy donor, from which energy can be transferred to an acceptor Eu^{3+}.

Cathodoluminescence Properties. Similar to the emission under UV excitation, the $TbBO_3$ and $TbBO_3$:1%Eu^{3+} samples also exhibit strong green and yellow light, respectively, upon excitation with an electron beam (accelerating voltage = 3 kV; filament current = 102 mA). Typical emission spectra are shown in parts a and b of Figure 12, respectively. For

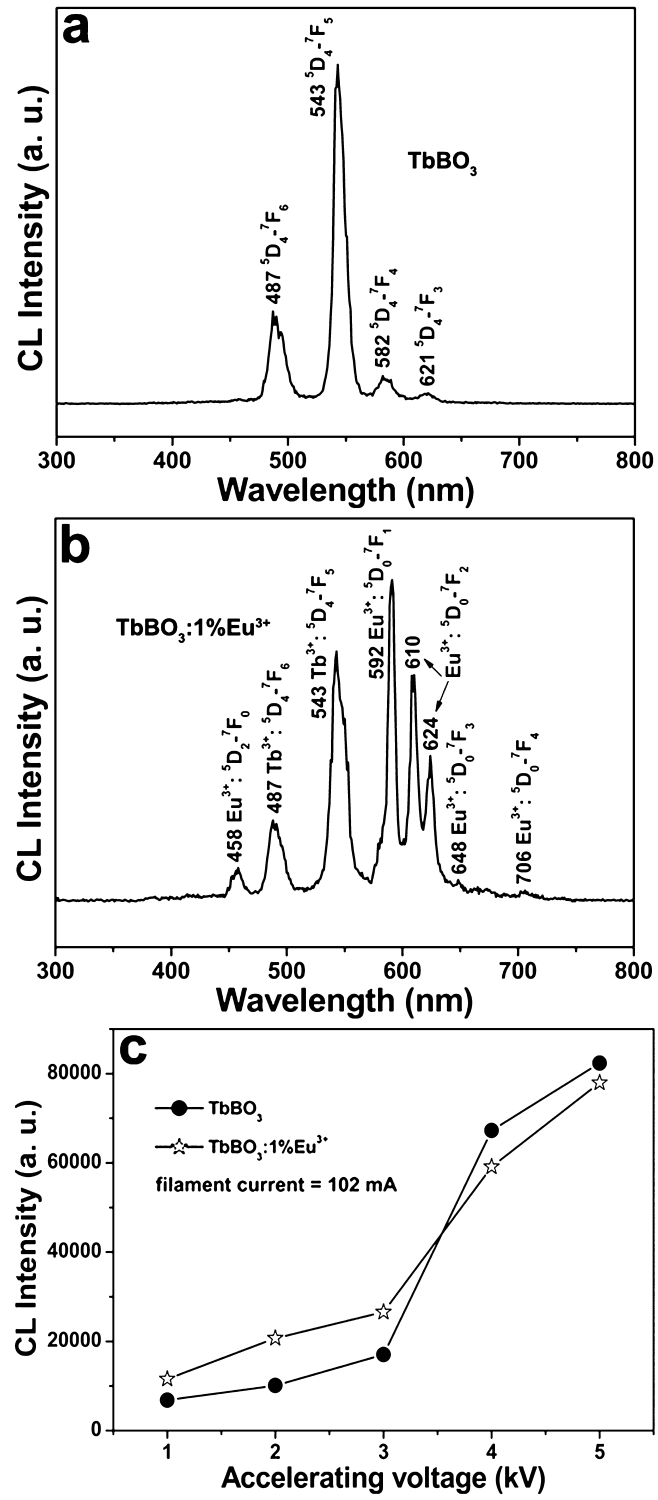

Figure 12. Typical cathodoluminescence spectra of the $TbBO_3$ (a) and $TbBO_3$:1%Eu^{3+} (b) (accelerating voltage = 3 kV; filament current = 102 mA) and the CL intensity of the $TbBO_3$ and $TbBO_3$:1%Eu^{3+} samples as a function of accelerating voltage (c).

the undoped $TbBO_3$, the CL emission spectrum (part a of Figure 12) is basically identical with the PL spectrum (part b of Figure 4). However, for $TbBO_3$:1%Eu^{3+} sample, the CL spectrum (part b of Figure 12) shows great difference with the PL spectrum (part d of Figure 4), that is, strong Tb^{3+} emission is still observed in the former besides the strong Eu^{3+} emission, whereas in the latter only the Eu^{3+} is

presented due to an efficient energy transfer from Tb^{3+} to Eu^{3+} (the Tb^{3+} emission can be neglected, part d of Figure 4). That is to say, the efficient energy transfer from Tb^{3+} to Eu^{3+} has not occurred in $TbBO_3$:1% Eu^{3+} under the excitation of electron beams. This is not surprising in view of the different CL mechanism from the PL one.[17] In PL, the UV and/or visible light is used to excite luminescent materials. The energy of these photons are only around 4∼6 eV. However, for CL, the energy of fast electrons under the acceleration of anode voltage can be tuned from a few thousands to thousands of electronvolts. So, the excitation energy on a single particle is much larger in CL than that in PL. The UV and/or visible usually excite the dopant ions (activator or sensitizer) directly (so the energy transfer process can occur and be identified). However, the fast electrons as a high-energy particle always excite the host lattice. After penetrating into the host lattice of a luminescent material, the fast primary electrons will give ionization. This ionization creates many secondary electrons. These secondary electrons can also give ionization and create many secondary electrons. These secondary electrons excite the host lattice and create many electron−hole pairs, leading to the formation of bound excitons.[18] These excitons, if formed, decay nonradiatively through a resonant or quasi-resonant transfer to the 4f shell of Tb^{3+} and/or Eu^{3+} ions and give their characteristic emissions. As a result, the energy transfer from Tb^{3+} to Eu^{3+} can be neglected in the CL process, and they show their own luminescence respectively excited by the electrons.

The CL intensity for the $TbBO_3$ and $TbBO_3$:1%Eu^{3+} samples were investigated as a function of accelerating voltage, as shown in part c of Figure 12. When the filament is fixed at 102 mA, the CL intensities of the $TbBO_3$ and $TbBO_3$:1%Eu^{3+} samples increase upon raising the acceleration voltage from 1 to 5 kV. Remarkablely, the CL intensity seems to jump at $V = 4$ kV and shows nonlinear relationship as a function of accelerating voltage, which might be related to the specific structure of each sample and the dependence of sensitivity of CL intensity on quite a few unexpected foreign factors.[9a,19] For cathodoluminescence, the Tb^{3+} and Eu^{3+} ions are excited by the plasmons produced by the incident electrons. The electron penetration depth can be estimated by equation

$$L[\text{Å}] = 250(A/\rho)(E/Z^{1/2})^n \quad (1)$$

where $n = 1.2/(1 - 0.29 \log_{10}Z)$, and A is the atomic weight, ρ is the density, Z is the atomic number, and E is the accelerating voltage (kV).[20] For $TbBO_3$:$x$$Eu^{3+}$, the electron penetration depth at 2 kV is 18.6 nm. This value is within the thickness of the $TbBO_3$:1%Eu^{3+} nanosheet observed from SEM (part b of Figure 3). With the increase of accelerating voltage, more plasmons will be produced by the incident electrons, which results in more Tb^{3+} and Eu^{3+} ions being excited and thus a higher CL intensity. The increase in electron energy is attributed to deeper penetration of the electron into the sample, which is governed by eq 1. The deeper penetration of electrons into the sample results in an increase in the electron−solid interaction volume in which excitation of Tb^{3+} and Eu^{3+} ions, which is responsible for light emission, takes place. Therefore, an increase in interaction volume, which effectively determines the generation of light inside the sample, with an increase in electron energy brings about an increase in the CL brightness of the $TbBO_3$:$x$$Eu^{3+}$ samples.[21]

4. Conclusions

In summary, we have demonstrated that a simple and mild hydrothermal method for synthesis of $Tb_{(1-x)}BO_3$:$x$$Eu^{3+}$ ($x = 0-1$) microsphere phosphors directly without further sintering treatment and reductive ambience for protection. An efficient energy transfer can occur from Tb^{3+} to Eu^{3+} in $TbBO_3$ host for the first time, which is ascribed to the energy overlap between Tb^{3+} and Eu^{3+} (Tb^{3+}:$^5D_4 \rightarrow {}^7F_{6,\,5,\,4,\,3} \rightleftarrows$ Eu^{3+}:$^7F_{0,\,1} \rightarrow {}^5D_{0,\,1,\,2} + \Delta E$) and hexagonal crystal structure of $TbBO_3$ host. By controlling the doping concentration of Eu^{3+} ($x = 0-1$%), the luminescent color could be modified from green, yellow, orange, to red-orange easily due to different composition of emissions of Tb^{3+}, and Eu^{3+} resulted from different energy efficiency at different doping concentration of Eu^{3+}. The CL spectrum of $TbBO_3$:1%Eu^{3+} shows great difference with the PL spectrum due to the different mechanism between CL and PL process. The study opens a novel pathway for tuning the luminescence properties by energy transfer and excitation sources.

Acknowledgment. This project is financially supported by the foundation of "Bairen Jihua" of Chinese Academy of Sciences, the MOST of China (No. 2003CB314707, 2007CB935502), and the National Natural Science Foundation of China (50572103, 20431030, and 00610227).

IC800586N

(17) Liu, X. M.; Lin, J. *J. Mater. Chem.* **2008**, *18*, 221.
(18) Diallo, P. T.; Boutinaud, P.; Mahiou, R.; Caperaa, J.; Cousseins, J. C. *Phys. Status Solidi A* **1997**, *160*, 255.
(19) (a) Yang, J.; Quan, Z. W.; Kong, D. Y.; Liu, X. M.; Lin, J. *Cryst. Growth Des.* **2007**, *7*, 730. (b) Yang, J.; Li, C. X.; Cheng, Z. Y.; Zhang, X. M.; Quan, Z. W.; Zhang, C. M.; Lin, J. *J. Phys. Chem. C* **2007**, *111*, 18148. (c) Liu, X. M.; Lin, J. *J. Phys. Chem. C* **2007**, *111*, 16601. (d) Liu, X. M.; Lin, C. K.; Luo, Y.; Lin, J. *J. Electrochem. Soc.* **2007**, *154*, J21. (e) Liu, X. M.; Pang, R.; Quan, Z. W.; Yang, J.; Lin, J. *J. Electrochem. Soc.* **2007**, *154*, J185. (f) Lee, Y. H.; Song, M. H.; Ju, B. K.; Shin, D. K.; Oh, M. H. *J. Vac. Sci. Technol., B* **1997**, *15*, 512. (g) Vecht, A.; Smith, D. W.; Chadha, S. S.; Gibbans, C. S. *J. Vac. Sci. Technol., B* **1994**, *12*, 781. (h) Wei, J.; Zhang, B. L.; Yao, N.; Wang, X. P.; Ma, H. Z.; Wang, S. M. *J. Vac. Sci. Technol., B* **2001**, *19*, 1082.
(20) Feldman, C. *Phys. Rev.* **1960**, *117*, 455.
(21) Kumar, D.; Cho, K. G.; Chen, Z.; Craciun, V.; Holloway, P. H.; Singh, R. K. *Phys. Rev. B* **1999**, *60*, 13331.